

# 基于双通道反射式微纳光纤耦合器膜片的精准连续血压监测

邹雪<sup>1,2</sup>, 范俊豪<sup>2</sup>, 罗彬彬<sup>2\*</sup>, 周富民<sup>2</sup>, 吴德操<sup>2</sup>, 张祖凡<sup>1</sup>, 赵明富<sup>2</sup>

<sup>1</sup>重庆邮电大学通信与信息工程学院, 重庆 400065;

<sup>2</sup>重庆理工大学光纤传感与光电检测重庆市重点实验室, 重庆 400054

**摘要** 提出一种反射式微纳光纤耦合器传感膜片, 以实现高精度、连续和无创血压监测。该传感膜片由反射式微纳光纤耦合器、聚二甲基硅氧烷薄膜和环氧树脂基底组成, 具有很高的压力灵敏度 ( $-0.682 \text{ kPa}^{-1}$ ), 且无需精确空间对准即可实现脉搏波检测; 然后, 构建双通道脉搏波检测系统, 以获得肱动脉传导时间、桡动脉传导时间以及桡动脉和肱动脉之间的传导时间差值; 基于上述参量, 利用支持向量回归算法建立血压预测模型。实验结果表明, 所提系统的收缩压平均偏差和标准偏差分别为  $0.08 \text{ mmHg}$  和  $1.13 \text{ mmHg}$ , 舒张压的平均偏差和标准偏差分别为  $-0.35 \text{ mmHg}$  和  $1.25 \text{ mmHg}$ , 符合美国医学仪器促进协会的标准, 与其他类型的传感器相比, 所提系统的准确度有明显提高。使用该系统监测一天内以及运动时的血压波动, 结果表明该系统在连续精准测量血压方面具有可行性及很大的应用潜力。

**关键词** 传感器; 血压监测; 微纳光纤耦合器; 人体脉搏波; 支持向量回归

中图分类号 TN253

文献标志码 A

DOI: 10.3788/AOS231738

## 1 引言

心血管疾病在人们的生活中越来越常见, 是威胁人类健康的最重要因素之一。据报道, 全球有超过 13 亿人患有心血管疾病, 心血管疾病导致的死亡人数从 1990 年的 1210 万增至 2019 年的 1860 万, 预计到 2030 年, 死亡人数将增至 2300 万<sup>[1-4]</sup>。血压 (BP) 是评价人体生理健康状况的重要生理参数, 可用于心血管疾病的早期诊断和预警。因此, 持续、精准地监测人体血压非常重要<sup>[5]</sup>。目前, 商用血压计通常采用充气袖带技术, 根据减压时袖带压力振荡波的振幅变化包络来测定血压, 但它存在测量者不适和无法连续测量的缺点<sup>[6]</sup>。近年来, 研究者提出了多种血压监测方法, 包括超声技术、光电容积描记法 (PPG) 等<sup>[7]</sup>。2018 年, Wang 等<sup>[8]</sup>提出一种检测人体动脉和静脉血流的超声设备, 可对心血管疾病进行实时连续监测。2013 年, Kurylyak 等<sup>[9]</sup>通过 PPG 传感器从人体脉搏信号中提取了 21 个特征, 并利用人工神经网络 (ANN) 实现了连续血压测量。2019 年, Mousavi 等<sup>[10]</sup>提出一种新算法, 该算法根据整体 PPG 信号预测血压, 而不考虑其参数特征, 提高了血压检测的准确性。2021 年, Byfield

等<sup>[11]</sup>利用双通道 PPG 传感器测量脉搏波速度, 基于机器学习模型实现了连续、准确的血压测量。然而, PPG 传感器的检测精度受检测环境的影响较大, 当人体肤色加深、皮肤出汗时, PPG 传感器的检测精度会降低。此外, 由于电磁干扰, 这些传感器无法监测复杂电磁环境 (如核磁共振) 中的脉搏波。

光纤传感器因其抗电磁干扰、灵敏度高、易于制造、结构紧凑和成本低廉等优点被用于连续和可穿戴式血压监测。由于脉搏传导时间 (PTT) 和脉搏波速度 (PWV) 与人类心血管疾病密切相关, 基于 PTT 和 PWV 预测血压的数学模型被认为是有效的。2016 年, Koyama 等<sup>[12]</sup>提出一种光纤 Bragg 光栅 (FBG) 血压监测系统, 通过检测人体右侧桡动脉脉搏波预测血压。2019 年, Haseda 等<sup>[13]</sup>使用 FBG 传感器监测人体肱动脉脉搏波, 该方法测量的血压值与商用血压计测量的参考值具有适度的相关性 (相关系数  $R=0.72$ )。2021 年, Kumar 等<sup>[14]</sup>进一步提出血压预测模型, 用于预测人体收缩压 (SBP) 和舒张压 (DBP), 二者的平均预测准确率分别为  $89.85\%$  和  $94.20\%$ 。2021 年, Li 等<sup>[15]</sup>利用光纤法布里-珀罗 (F-P) 腔传感器检测人体腕部桡动脉的脉搏波形, 并根据脉搏信号得出的 PTT 建立了血压

收稿日期: 2023-11-03; 修回日期: 2023-12-06; 录用日期: 2023-12-13; 网络首发日期: 2023-12-23

基金项目: 重庆英才青年拔尖人才计划 (cstc2021ycjh-bgzxm0128)、重庆英才创新领军人才计划 (CSTC2021YCYJH-BGZXM0287)、重庆市自然科学基金创新与发展联合基金 (CSTB2023NSCQ-LZX0008)、重庆理工大学科研创新团队培育计划 (2023TDZ002)、重庆理工大学研究生科研创新项目 (gzlxc20232042)

通信作者: \*luobinbin@cqut.edu.cn

预测模型。2022年, Li等<sup>[16]</sup>专门设计用于检测人体桡动脉的微光纤封装结构, 该传感器无需严格的对准要求即可快速准确地捕捉人体脉搏信号。然而, 这些光纤传感器普遍都是单通道的, 模型精度不够高。为进一步提高模型预测的准确率, Pang等<sup>[17]</sup>利用单模-多模-单模光纤结构同时测量肱动脉传导时间(BPTT)和桡动脉传导时间(RPTT), 然后根据桡动脉和肱动脉的传导时间差(DBRPTT)实现血压的连续测量, 该方法的检测灵敏度依赖于脉搏波位置的精准对齐, 且其采用透射式光路, 因此传感器集成的结构不够紧凑, 实际使用不太方便。

本文提出一种基于双通道反射式微纳光纤耦合器(R-OMC)膜片结构的高精度血压监测方法。微纳光纤耦合器(OMC)<sup>[18]</sup>在检测脉搏波时的形变主要由轴向应变和弯曲应变引起, 其轴向应变灵敏度约比相同直径的单根微纳光纤高两倍<sup>[19-20]</sup>。利用特殊封装结构的R-OMC膜片监测人体脉搏波信号, 可有效提高检测灵敏度, 并可降低传感器与人体动脉之间严格的对准要求。然后, 利用双通道R-OMC膜片从8名志愿者的肱动脉和桡动脉采样的大量脉搏信号中提取

BPTT、RPTT和DBRPTT, 使用支持向量回归(SVR)模型实现连续、准确的血压预测。

## 2 传感器原理与特性

### 2.1 传感器结构设计与制备

R-OMC由锥区和腰区组成, 其中腰区处的两条微纳光纤平行紧密地叠加在一起, 如图1(a)所示, 入射光通过P1端口输入, 同时被激发的偶模和奇模两种模式沿腰区传输并在端面反射, 最后由端口P2输出形成干涉光谱<sup>[20]</sup>。由于腰区的强倏逝场特性, R-OMC的传输光强对压力非常敏感, 当对腰区施加压力时, R-OMC会发生轻微弯曲, 导致导波模式转变为辐射模式, 从而造成光能量损失。采用火焰熔融拉锥法制造R-OMC, 两根单模光纤在被剥离涂敷层后相互缠绕2~3圈, 利用光纤拉锥机将其拉制成透射型光纤耦合器(T-OMC), 然后采用高精度光纤切割器切割T-OMC的腰部区域, 得到端面光滑平整的R-OMC, 以减小光在端面的散射干扰, 同时增强光反射效应。如图1(b)所示, 所制备的R-OMC腰区区域直径为5  $\mu\text{m}$ , 长度为10 mm。

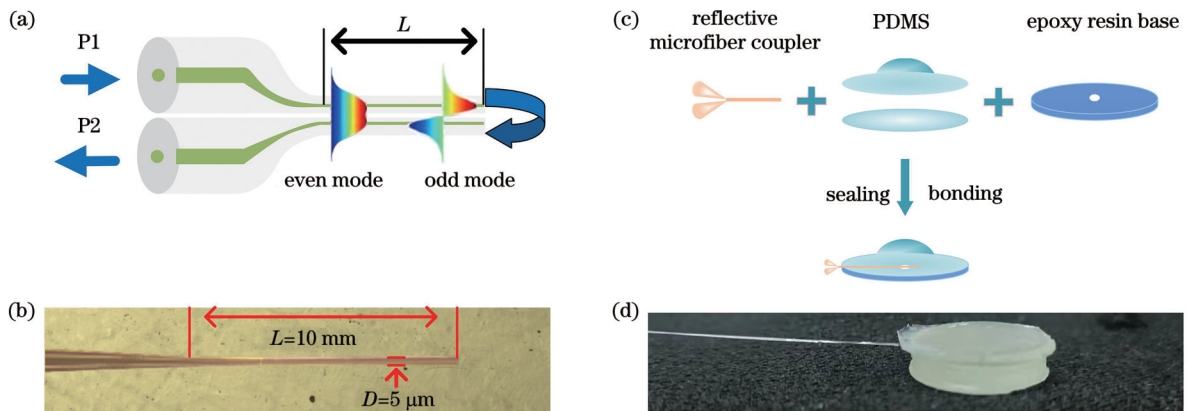


图1 结构示意图。(a) R-OMC的结构;(b)显微镜下的R-OMC;(c)传感器膜片的结构;(d)完整的传感器膜片

Fig. 1 Diagram of structure. (a) Structure of R-OMC; (b) R-OMC under microscope; (c) structure of sensor chip; (d) complete sensor chip

为保护制备好的R-OMC波导结构, 首先将其浸泡在特氟龙溶液10 min, 然后放入干燥箱中在80  $^{\circ}\text{C}$ 下干燥30 min, 以使腰区表面和端面都覆盖一层特氟龙薄膜。如图1(c)所示, 反射式微纳光纤耦合器传感膜片(R-OMCSC)由一个R-OMC、一个环氧树脂基底和两层固态PDMS组成。聚二甲基硅氧烷(PDMS)层由液态PDMS固化成型制备而成, 底层是直径为15 mm、厚度为50  $\mu\text{m}$ 的圆形薄膜, 覆盖层是直径为15 mm、厚度为100  $\mu\text{m}$ 的圆形底座和直径为10 mm、高度为1.5 mm的凸起球形结构。由于PDMS的折射率低(RI约为1.4)、耐热性和耐水性好, 且易于和人体皮肤贴合, 柔性PDMS薄膜不仅能保护光纤微结构, 减少温度和湿度等外部环境的影响, 还能确保外部刺激准确地传递到整个传感器表面, 因此, 封装后的R-OMC可

用作压力传感器来监测人体脉搏振动信号。环氧树脂基底由光固化3D打印机打印制作, 直径为15 mm, 厚度为5 mm, 基底中心有一个直径为1 mm的圆形通孔。传感器各部分制备完成后, 将R-OMC放在两层PDMS的中间, 由于范德瓦耳斯力的作用, 两层PDMS紧密贴合, 形成三明治结构, 再将夹层结构连接到环氧树脂基底上, 基底上涂覆了一层液态PDMS。最后, 为了确保整个结构的密封性, 将其放入85  $^{\circ}\text{C}$ 的烤箱中烘烤20 min, 以获得完整的R-OMCSC结构, 如图1(d)所示。

### 2.2 传感器结构力学仿真

使用ABAQUS CAE软件对传感器封装结构进行力学仿真, 以验证该设计对提高灵敏度和减小传感器对空间位置敏感性的影响。建立如图2(a)所示的仿

真模型,当凸面球形结构受到来自各个方向的压力时,R-OMC所在的平面会产生垂直位移,从而模拟压力检测状态。在底座上的通孔位置,R-OMC比其他位置有更大的弯曲和更多的光强损耗,因此能有效提高传感器对压力的灵敏度。在该模型中,PDMS采用超弹性材料的Mooney-Rivlin模型,并将材料的特性转换为三个参数: $C_{10}=0.243243$ , $C_{01}=0.060811$ , $d=0.133333$ ,其中: $C_{10}$ 和 $C_{01}$ 是PDMS材料参数,分别表示主方向上应力和应变的弹性模量; $d$ 为体积模量,表示固体材料在体积变化时的抗压能力。环氧树脂的杨氏模量为1 GPa,泊松比为0.38<sup>[21-22]</sup>。此外,在球形结构的

不同位置施加压力,以探索通孔平面的垂直位移与所施压力之间的关系,如图2(b)所示,压力设定为1 kPa,以模拟人体脉搏压力。在图3中,偏移量为0 mm表示在球面中心施加压力,使该位置的平面通孔位移最大为350  $\mu\text{m}$ ,且各位置的垂直位移是对称的;偏移量(1、2、3、4 mm)表示施加的压力位置与球面中心的距离,通孔位置的位移会随着偏移量的增加而逐渐减小,在通孔平面靠近施加压力的一侧,位移值会大于另一侧。当偏移量为4 mm时,通孔的平面位移(100  $\mu\text{m}$ )比偏移量为0 mm时衰减了约70%,但由于传感器的高灵敏度特性,在此位置仍能检测到脉冲信号,所设计的封装结构可降低R-OMC对检测位置的依赖性<sup>[23]</sup>。

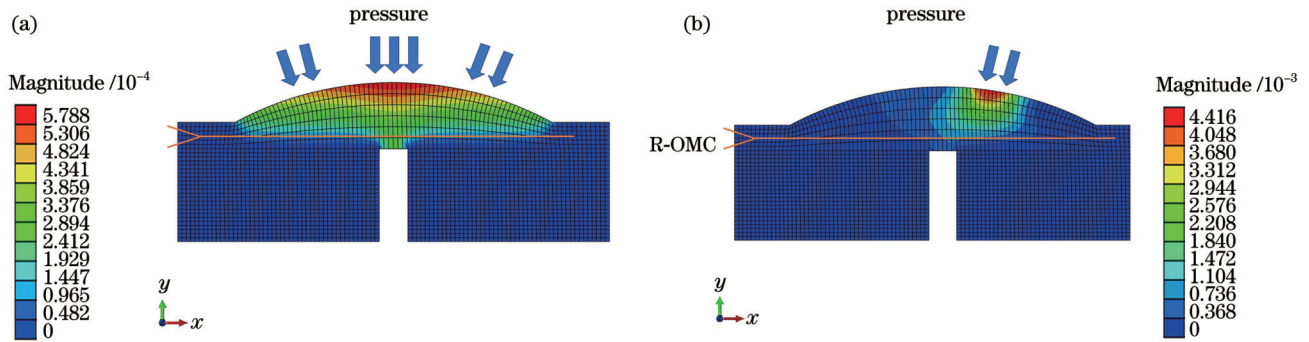


图2 封装结构的机械模拟。(a)来自多个方向的压力;(b)来自单个方向的压力

Fig. 2 Mechanical simulation of package structure. (a) Pressure from multiple directions; (b) pressure from single direction

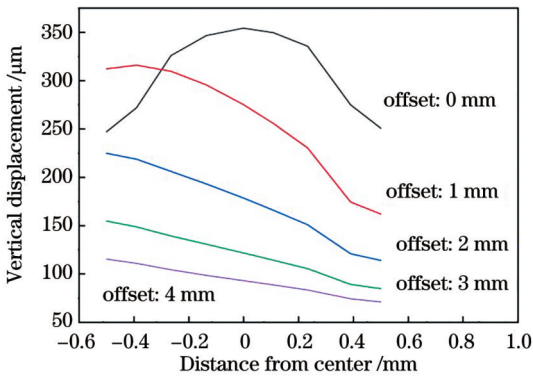


图3 PDMS底层的垂直位移

Fig. 3 Vertical displacement of bottom layer of PDMS

### 2.3 传感器的压力传感性能分析

为评估R-OMCSC的灵敏度,搭建如图4所示的检测系统,该系统由可调谐激光光源(TLS)、隔离器、光电探测器(PD)、高精度三维微位移测试平台(ESM30)和示波器组成。波长为1550 nm的激光光源通过隔离器和R-OMCSC后,被PD转换成电信号,最后以电压的形式显示在示波器上。这里采用隔离器能有效阻隔传感器端面的反射光进入光源。如图4中插图所示,在传感器球形结构的中心施加不同的压力,观察示波器的电压变化。传感器的灵敏度( $S$ )由电压变化( $\Delta V/V_0$ )与外加压力( $P$ )的斜率定义,即 $S =$

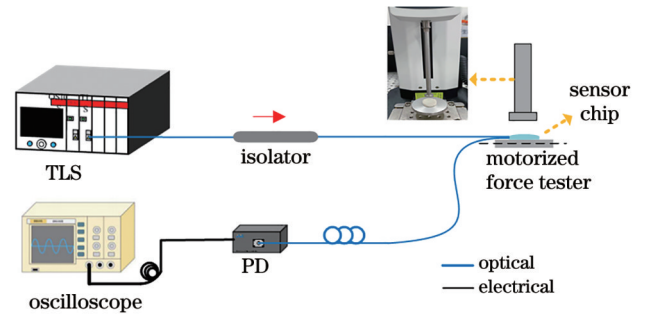


图4 基于R-OMCSC的性能测试系统

Fig. 4 Testing system for performance of R-OMCSC

( $\Delta V/V_0$ )/ $\Delta P$ ,其中, $\Delta V$ 、 $V_0$ 和 $\Delta P$ 分别是电压变化、无负载电压和外加压力变化<sup>[13]</sup>。测试结果如图5(a)所示,电压的变化随着施加压力的增加而增加,在约5 kPa时电压下降到约0,但由于人体桡动脉和肱动脉的脉压一般为500~1000 Pa<sup>[24]</sup>,因此传感器在此范围内的检测灵敏度较高( $-0.682 \text{ kPa}^{-1}$ ),可以有效地检测到脉搏信号。通过在传感器球形结构的不同位置施加1 kPa压力,模拟脉冲信号与传感器不同空间位置的配准,结果如图5(b)所示,随着施加压力的偏移量增加,电压的变化逐渐减小,但当偏移量为3 mm时,传感器仍有响应。为了评估响应时间,用电动位移平台对传感器膜片施加垂直向下1 N的力。压力响应如图5(c)所示,在加载和卸载压力的瞬间,传感器膜

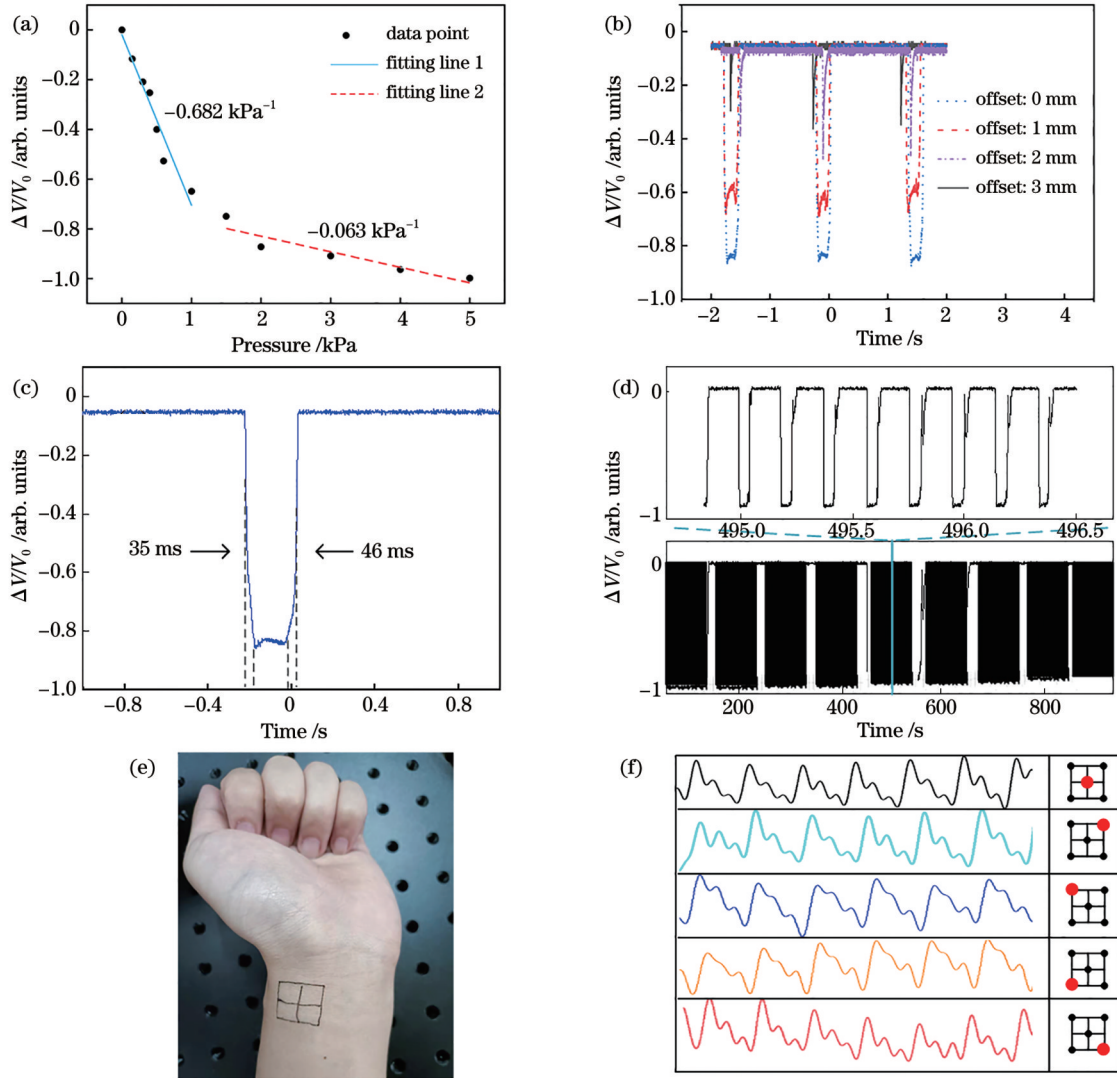


图5 R-OMCSC的特性。(a)压力灵敏度;(b)施加在不同位置的压力的电压变化;(c)响应时间;(d)重复性;(e)桡动脉的不同检测位置;(f)人体脉搏在不同位置的脉搏波形

Fig. 5 Characteristics of R-OMCSC. (a) Pressure sensitivity; (b) voltage change of pressure applied at different locations; (c) response time; (d) repeatability; (e) different detection locations in radial artery; (f) pulse waves at different locations of human pulse

片都能立即做出响应,响应时间分别为 35 ms 和 46 ms,因此,该传感器可以满足实时检测人体脉搏波信号的要求。此外,进一步验证传感器的耐用性和可重复性,将 R-OMCSC 连接到高频振动台(ECS-1028)上,振动台持续对 R-OMCSC 施加频率为 5 Hz、大小为 1 N 的周期性压力,其重复压力响应如图 5(d)所示,在 2500 次循环后,传感器仍表现出良好的压力响应,重复性极佳,但约 5000 次循环后,传感器膜片的压力响应幅度比开始时下降了约 5%,随着循环次数的增加,传感器响应呈微弱下降趋势,即响应的标准偏差会略有增加,这种现象可能是由于 PDMS 薄膜在经过数千次压力循环后弹性滞后以及振动台的误差造成,但后续的血压预测主要依靠短时脉搏信号的时间特性,R-OMCSC 测量脉搏的时间较短(约 5 s),短时间内的响应几乎相同,因此这段时间内的标准偏差很小。上述结果表明,R-OMCSC 具有快速响应和良好的耐用性。

如图 5(e)所示,将传感器放置在边长为 15 mm 的人体脉搏区域的不同位置,结果如图 5(f)所示,传感器在 4 个子方格的不同位置都能有效检测到高保真脉搏信号,因此可保证传感器响应对脉搏检测区域没有严格的对准要求。

### 3 实验与建模

#### 3.1 双通道脉搏波检测

脉搏波信号包含许多特征参数,如 PTT、PWV、波形等,反映人体心血管功能和血液传输过程中丰富的生理信息<sup>[25]</sup>。人体手臂肱动脉和桡动脉的典型脉搏波形如图 6 所示,通过计算叩击波和二尖瓣波两处脉搏峰的时间点,可以得到与血压相关的三个参数: BPTT、RPTT、DBRPTT<sup>[26]</sup>,其中 BPTT 和 RPTT 分别定义为肱动脉和桡动脉脉搏信号的叩击波与二尖瓣波之间的时间差,DBRPTT 则定义为同时测量的两个

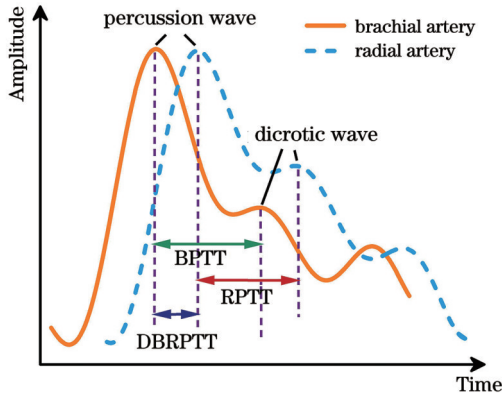


图 6 肱动脉和桡动脉的典型脉搏波形

Fig. 6 Typical pulse waveform of brachial artery and radial artery

动脉脉搏信号的两个二尖瓣波之间的时间差。

如图 7 所示,用紫外(UV)胶将 R-OMCSC 粘贴在弹性腕带的内侧中心,使传感器稳定、准确地接触人体动脉,从而提高检测的稳定性和灵敏度。双通道脉搏波检测系统与 2.3 节中测试系统类似,由一个 TLS、两个隔离器、两个 PD 和一个示波器组成。TLS 的两路输出激光设置为相同波长(1560 nm),分别作为肱动脉和桡动脉的 R-OMCSC 脉搏传感器的输入光。实验中选取 8 名健康志愿者(4 名男性,年龄分别为 25 岁、24 岁、52 岁和 60 岁;4 名女性,年龄分别为 25 岁、30 岁、55 岁和 60 岁)采集脉搏数据。

脉搏波的采集由两个带 R-OMCSC 的腕带和一个商用血压计完成,采样持续 10 天,每天 8:00 至 21:00 每小时采集一次脉搏样本,共采集 14 个样本。实验中,志愿者直立坐着,双手平放在测试台上,与心脏保持同一水平,以提高测量的准确性,将两条带有 R-OMCSC 的弹性腕带分别固定于志愿者左臂的桡动脉和肱动脉,如图 7 所示。将商用血压计(YE-680)置于左上臂测量血压,该血压值代表血压的真实值。当商用血压计测量血压时,示波器会同时存储两个 R-OMCSC 弹性腕带检测到的脉搏波,最后得到 1120 组数据,这些数据由脉搏波形和其对应的血压值组成。

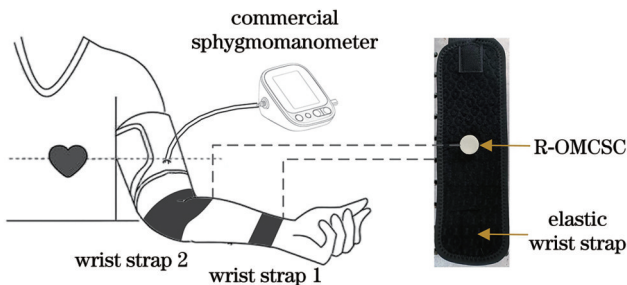


图 7 双通道脉搏波检测方法

Fig. 7 Dual-channel pulse wave detection method

### 3.2 脉搏数据的 PTT 提取

对所采集到的 1120 组数据进行预处理和特征提取,如图 8 所示,首先通过小波分解去除原始信号的基线干扰,并通过低通滤波去除高频噪声,然后采用峰值搜索法搜索叩击波和二尖瓣波的位置,最后计算脉搏波的 PTT。为了使计算结果更加准确,计算了同一组脉搏信号中 5 个连续脉搏波的 PTT,然后将每个 PTT 的平均值作为最终的 PTT 值,用于表征整组信号。

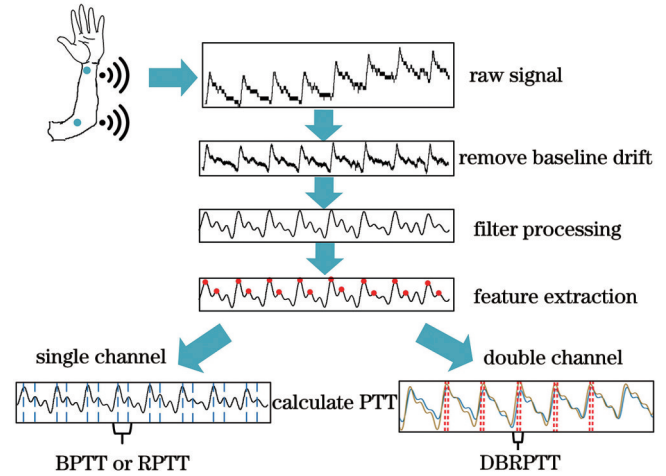


图 8 脉搏波预处理过程

Fig. 8 Pulse wave preprocessing process

PTT 被认为是通过脉搏波预测血压的有效方法,其关系<sup>[15]</sup>可表示为

$$B_p = K_a \ln P_{TT} + K_b \frac{1}{P_{TT}^2} + K_c, \quad (1)$$

式中:  $B_p$  表示 SBP 或 DBP;  $P_{TT}$  表示 RPTT、BPTT 或 DBRPTT;  $K_a$ 、 $K_b$ 、 $K_c$  表示与个体相关的系数,可通过建立血压参考值和实验得出的 PTT 值之间的函数关系来获得。所测得 1120 组脉搏信号的  $P_{TT}$  有一定的波动范围,如表 1 所示,三组  $P_{TT}$  的最大值分别为 282 ms、270 ms 和 90 ms,最小值分别为 230 ms、217 ms 和 25 ms。此外,三组  $P_{TT}$  均与血压呈负相关,根据式(1),SBP 和 DBP 会随着  $P_{TT}$  值的增加而降低。为了更准确地表示人体真实的  $P_{TT}$  值,定义了  $K$  值来表示脉搏波传导时间的长短,首先将三种  $P_{TT}$  值进行归一化,将其最大值归为 1,最小值归为 0,然后通过计算三组归一化  $P_{TT}$  值的平均值得到  $K$  值,其取值范围为 0 至 1。与单一的  $P_{TT}$  相比, $K$  值同时考虑了肱动脉和桡动脉脉搏信号的影响,因此能更有效地反映血压的真实水平。

表 1 RPTT、BPTT 和 DBRPTT 值的测量范围  
Table 1 Measurement range of RPTT, BPTT, and DBRPTT

Parameter	RPTT / BPTT / DBRPTT /			Normalization
	ms	ms	ms	
Maximum	282	270	90	1
Minimum	230	217	25	0

### 3.3 血压预测模型

支持向量回归(SVR)是一种二元分类模型回归算法,在非线性和样本量较小的情况具有泛化能力好、预测准确率高等优点<sup>[27]</sup>。本研究中 $K$ 值预测血压是一个非线性回归问题,针对本实验的1120组样本数据,选择SVR建立血压预测模型是合理有效的。

$K$ 值和商用血压计对应血压值作为一个数组 $\{(x_i, y_i), i = 1, 2, \dots, n\}$ ,使用非线性映射将数据映射到多维特征空间的特征上,将回归问题转化为线性问题<sup>[17]</sup>:

$$f(x) = \sum_{i=1}^n (\alpha_i - \alpha_i^*) K \langle x_i, x_j \rangle + b, \quad (2)$$

式中: $\alpha_i$ 和 $\alpha_i^*$ 为拉格朗日乘子; $b$ 为待确定的模型参

数; $K \langle x_i, x_j \rangle$ 是径向基函数,可表示为

$$K \langle x_i, x_j \rangle = \exp \left( -g \|x_i - x_j\|^2 \right), \quad (3)$$

式中: $g$ 是SVR模型的核半径。惩罚系数 $c$ 和核半径 $g$ 是预测模型中的超参数,它们的设置对模型的预测精度有很大影响。针对上述样本值进行网格搜索以获得最佳设置值,图9(a)和(b)为志愿者SBP和DPB预测模型的网格搜索情况,其中, $x$ 坐标、 $y$ 坐标和 $z$ 坐标分别为 $\lg 2c$ 、 $\lg 2g$ 和均方误差(MSE)。最终确定SBP预测模型中 $c$ 和 $g$ 的设置参量分别为16和0.003512, DBP模型中 $c$ 和 $g$ 的设置参量分别为64和0.003528。

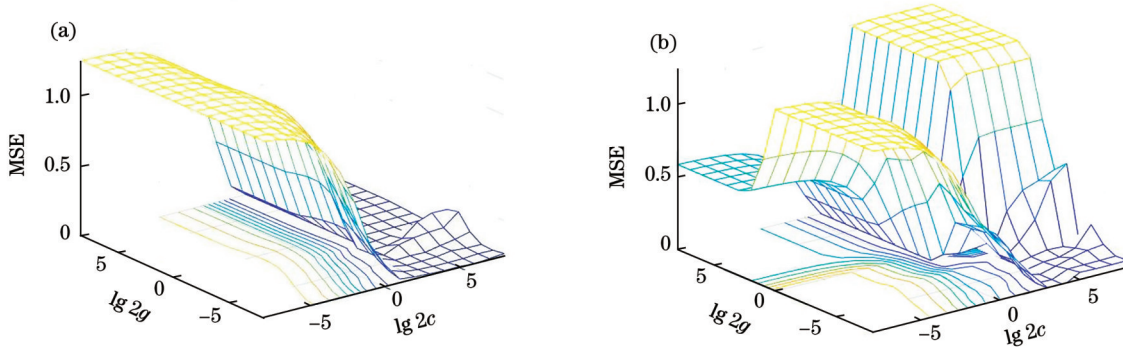


图9 对 $c$ 和 $g$ 进行网格搜索的结果。(a) SBP模型;(b) DBP模型  
Fig. 9 Grid search results for  $c$  and  $g$ . (a) SBP model; (b) DBP model

## 4 结果与讨论

将1120组脉搏和血压数据中90%的数据作为训练集输入SVR模型,剩余10%的数据作为测试集用

于验证模型的准确率。从测试集的模型输出结果中随机抽取25组数据,如图10所示,其中 $K$ 值与SVM模型输出的预测值和商用血压计的真实值一一对应,且呈负相关。

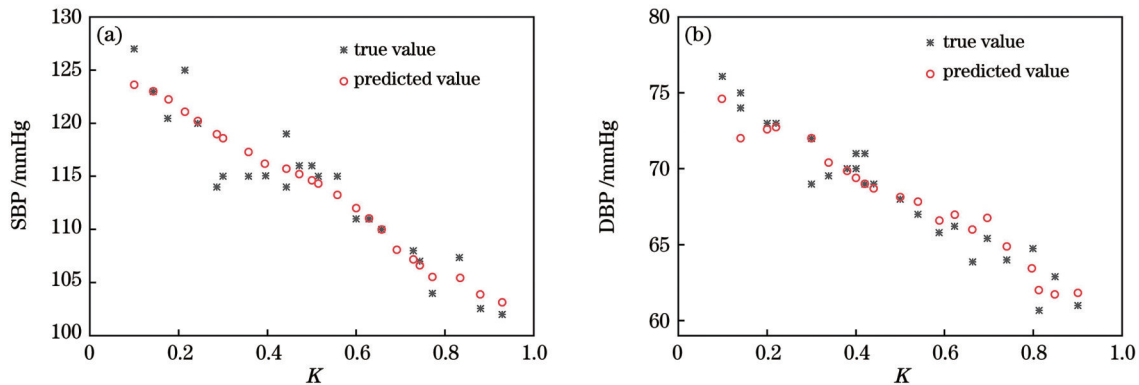


图10 SVR预测模型的输出。(a) SBP模型;(b) DBP模型  
Fig. 10 Output of SVR prediction model. (a) SBP model; (b) DBP model

如图11(a)、(b)所示,横轴和纵轴分别代表参考血压和预测血压,SBP和DBP的相关系数 $R$ 值分别为0.96和0.95,由此可见,参考值与预测值之间具有良好的正相关性。在图11(c)、(d)中,采用Bland-Altman图来评价商用血压计和SVR预测获得血压的一致性,横坐标是预测BP与参考BP的平均值,纵坐标是两者之间的差值,中间的实线是差值的平均值,绝对值越小

则一致性越好。图中两条虚线之间的区域为95%置信区间[平均值为 $\pm 1.96$ 标准差(SD)],可见,SBP的差值均值和SD值分别为0.08 mmHg和1.13 mmHg, DBP的差值均值和SD值分别为-0.35 mmHg和1.25 mmHg。对于SBP和DBP,在95%置信区间内的测试点越多,两种方法的一致性越好,这意味着基于SVR预测模型的方法能更有效地获得准确的血压。

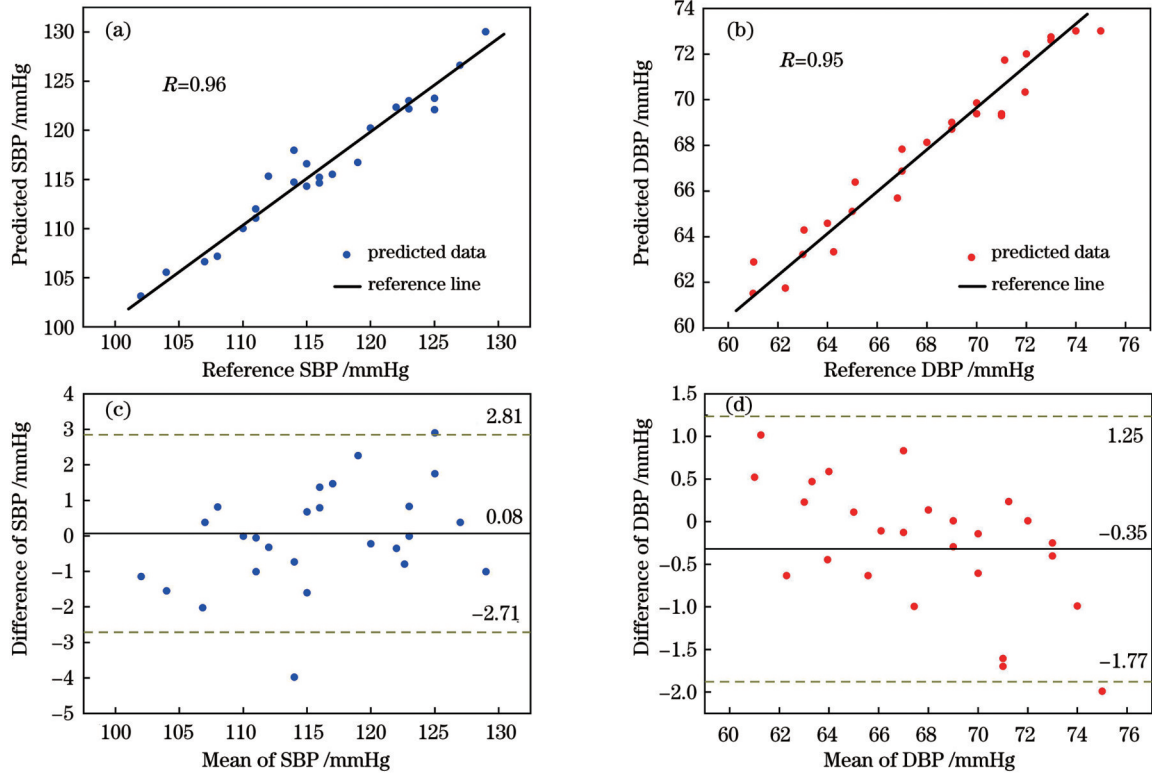


图 11 基于 SVR 的双通道血压检测模型的相关图和 Bland-Altman 图。(a)(c) SBP 模型; (b)(d) DBP 模型

Fig. 11 Correlation plots and Bland-Altman plots of dual-channel BP detection model based on SVR. (a)(c) SBP model; (b)(d) DBP model

表 2 中列出了近年来报道的血压传感器和本研究的性能,其中平均偏差(MD)和 SD 是 AAMI 提出的衡量血压测量准确性的两个关键指标,MD 表示预测血压与参考血压的平均值。本方案相比于其

他方法,传感器的灵敏度有一定程度的提高,响应时间均在毫秒量级,且 SBP 和 DBP 的预测准确度具有明显优势,相关指标均低于 AAMI 标准  $[(5 \pm 8) \text{ mmHg}]^{[28]}$ 。

表 2 与其他血压传感器的性能比较

Table 2 Performance comparison with other blood pressure sensors

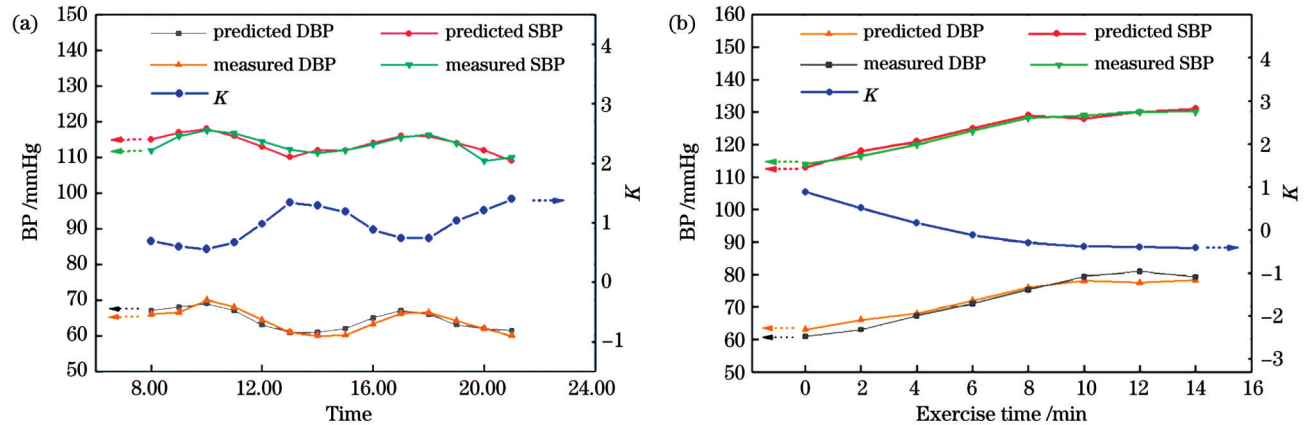
Sensor type	Sensor location	Pulse pressure sensitivity	Response time /ms	SBP accuracy (MD, SD)	DBP accuracy (MD, SD)	Reference
PPG	Finger tips	-	-	0.06, 7.08	0.01, 4.66	[29](2016)
OI	Face	-	-	0.39, 7.30	-0.20, 6.00	[30](2019)
OFCD	Radial artery	-	-	0.24, 2.39	0.12, 2.62	[15](2020)
AFMSC	Radial artery	-0.22	11	-	-	[16](2022)
AFOFD	Radial artery	-213 $\mu\text{W}/\text{kPa}$	5	-0.35, 4.68	-2.54, 4.07	[31](2023)
Double R-OMC	Radial artery, brachial artery	-0.682 $\text{kPa}^{-1}$	35	0.08, 1.13	-0.35, 1.25	This work

Notes: PPG represents photoplethysmograph, OI represents optical imaging, OFCD represents optical fiber composite diaphragm, AFMSC represents alignment-free microfiber-based sensor chip, AFOFD represents fiber adapter and liquid capsule.

为了进一步评估该传感器的可行性,选取了一名志愿者(女性,24岁)来分析血压测量趋势。图 12(a)显示了一天中从 8:00 到 21:00 的 14 组血压数据 SBP 和 DBP,可以看出,SBP 和 DBP 在上午时段和下午时段分别都有一个峰值,在中午时段有所下降。而 K 值的变化趋势与血压的变化趋势相反,验证了 K 值与血压呈负相关。这种“两峰一谷”的血压变化趋势广泛分

布于大多数正常人中,被称为勺状血压。事实上,当外周血管阻力和动脉壁僵硬发生变化时,血压  $P_{TT}$  值也会有规律地波动<sup>[32]</sup>。显然,本文提出的血压监测系统可以持续有效地监测血压的健康水平。

此外,为评估传感器监测运动中血压波动的稳定性,一名志愿者(男性,24岁)在做深蹲和慢跑的混合运动过程中接受了测试,总的测试时间为 14 min,每

图 12 血压和  $K$  值的变化。(a)一天内的不同时刻;(b)运动时Fig. 12 Changes of BP and  $K$  value. (a) Different times in one day; (b) exercise time

2 min 由该传感器记录一次血压,每次持续 10 s。如图 12(b)所示,随着运动时间的延长,SBP 和 DBP 均有所上升,但在约 10 min 后保持稳定, $K$  值与  $B_p$  值相反,其主要原因是运动时血管剧烈收缩并分泌血管紧张素,从而导致血压升高<sup>[33-34]</sup>。

实验结果表明,基于 R-OMCSC 的双通道腕带能够精确连续地获取人体脉搏信号,并通过 PTT 建立 SVR 模型,实现连续、准确的血压监测。与传统的电子血压检测传感器相比,本文提出的传感器的最大优点是抗电磁干扰,从而扩大了应用场景范围,其集成在腕带中还具有采集方便、灵敏度高等优点。

## 5 结 论

本文提出一种反射式微纳光纤耦合器传感膜片,用于准确、连续的血压监测和心血管健康评估。R-OMCSC 具有高灵敏度 ( $-0.682 \text{ kPa}^{-1}$ ) 和检测脉搏波时无需精准空间对齐的特点,通过将该传感器嵌入运动腕带,实现了人体肱动脉和桡动脉的脉搏波监测。然后,建立双通道脉搏波检测系统,以获得桡动脉和肱动脉的 RPTT、DPTT 和 DBRPT 值,并建立相应的 SVR 血压预测模型,通过关联图和 Bland-Altman 图讨论了该模型的准确性。实验结果表明,模型的 MD 值和 SD 值符合 AAMI 标准,SBP 值分别为  $0.08 \text{ mmHg}$  和  $1.13 \text{ mmHg}$ ,DBP 值分别为  $-0.35 \text{ mmHg}$  和  $1.25 \text{ mmHg}$ ,与其他类型的传感器相比,所提出的传感器检测的 SBP 和 DBP 在准确度上都有较大的提高,并可以实现连续的血压监测功能。后续工作可在几方面加以改进:1)可进一步进行系统光源、探测部分的集成化和微型化;2)通过增加检测对象的数量和类型来提高预测模型的准确性;3)进一步考虑其他脉搏特征,包括总外周阻力、动脉顺应性、脉搏容量等,从而使预测模型更加准确。该可穿戴式的双通道连续血压监测系统在人类心血管疾病预防领域将具有良好的应用潜力。

## 参 考 文 献

- [1] Chen W W, Gao R L, Liu L S, et al. China cardiovascular diseases report 2015: a summary[J]. *Journal of Geriatric Cardiology*: JGC, 2017, 14(1): 1-10.
- [2] Jonas M, Kazarski R, Chernin G. Ambulatory blood-pressure monitoring, antihypertensive therapy and the risk of fall injuries in elderly hypertensive patients[J]. *Journal of Geriatric Cardiology*, 2018, 15(4): 284-289.
- [3] Schumann B, Seidler A, Kluttig A, et al. Association of occupation with prevalent hypertension in an elderly East German population: an exploratory cross-sectional analysis[J]. *International Archives of Occupational and Environmental Health*, 2011, 84(4): 361-369.
- [4] Chaising S, Temdee P. Determining significant risk factors for preventing elderly people with hypertension from cardiovascular disease complication using maximum objective distance[J]. *Wireless Personal Communications*, 2020, 115(4): 3099-3122.
- [5] Berkemans G F N, Kuipers S, Westerhof B E, et al. Comparing volume-clamp method and intra-arterial blood pressure measurements in patients with atrial fibrillation admitted to the intensive or medium care unit[J]. *Journal of Clinical Monitoring and Computing*, 2018, 32(3): 439-446.
- [6] Teng X F, Zhang Y T. An evaluation of a PTT-based method for noninvasive and cuffless estimation of arterial blood pressure [C]//2006 International Conference of the IEEE Engineering in Medicine and Biology Society, August 30-September 3, 2006, New York, NY, USA. New York: IEEE Press, 2006: 6049-6052.
- [7] Allen J. Photoplethysmography and its application in clinical physiological measurement[J]. *Physiological Measurement*, 2007, 28(3): R1-R39.
- [8] Wang C H, Li X S, Hu H J, et al. Monitoring of the central blood pressure waveform via a conformal ultrasonic device[J]. *Nature Biomedical Engineering*, 2018, 2(9): 687-695.
- [9] Kurylyak Y, Lamonaca F, Grimaldi D. A neural network-based method for continuous blood pressure estimation from a PPG signal[C]//2013 IEEE International Instrumentation and Measurement Technology Conference (I2MTC), May 6-9, 2013, Minneapolis, MN, USA. New York: IEEE Press, 2013: 280-283.
- [10] Mousavi S S, Firouzmand M, Charmi M, et al. Blood pressure estimation from appropriate and inappropriate PPG signals using a whole-based method[J]. *Biomedical Signal Processing and Control*, 2019, 47: 196-206.
- [11] Byfield R, Miller M, Miles J, et al. Towards robust blood pressure estimation from pulse wave velocity measured by



- photoplethysmography sensors[J]. *IEEE Sensors Journal*, 2022, 22(3): 2475-2483.
- [12] Koyama S, Ishizawa H, Fujimoto K, et al. Influence of individual differences on the calculation method for FBG-type blood pressure sensors[J]. *Sensors*, 2016, 17(1): 48.
- [13] Haseda Y, Bonafacio J, Tam H Y, et al. Measurement of pulse wave signals and blood pressure by a plastic optical fiber FBG sensor[J]. *Sensors*, 2019, 19(23): 5088.
- [14] Kumar N V, Pant S, Sridhar S, et al. Fiber Bragg grating-based pulse monitoring device for real-time non-invasive blood pressure measurement: a feasibility study[J]. *IEEE Sensors Journal*, 2021, 21(7): 9179-9185.
- [15] Li L Y, Li Y P, Yang L Y, et al. Continuous and accurate blood pressure monitoring based on wearable optical fiber wristband[J]. *IEEE Sensors Journal*, 2021, 21(3): 3049-3057.
- [16] Li L Y, Liu Y F, Song C Y, et al. Wearable alignment-free microfiber-based sensor chip for precise vital signs monitoring and cardiovascular assessment[J]. *Advanced Fiber Materials*, 2022, 4(3): 475-486.
- [17] Pang Y N, Liu B, Liu J, et al. Singlemode-multimode-singlemode optical fiber sensor for accurate blood pressure monitoring[J]. *Journal of Lightwave Technology*, 2022, 40(13): 4443-4450.
- [18] 李玉洁, 罗彬彬, 邹雪, 等. 基于双螺旋微纳光纤耦合器的光学游标传感特性研究[J]. *中国激光*, 2023, 50(14): 1406001.  
Li Y J, Luo B B, Zou X, et al. Sensing characteristics of optical vernier of double-helix micro-nano optical fiber coupler[J]. *Chinese Journal of Lasers*, 2023, 50(14): 1406001.
- [19] Liu K J, Fan J H, Luo B B, et al. Highly sensitive vibration sensor based on the dispersion turning point microfiber Mach-Zehnder interferometer[J]. *Optics Express*, 2021, 29(21): 32983-32995.
- [20] 范俊豪, 杨祥文, 罗彬彬, 等. 基于色散拐点微纳光纤耦合器的通孔悬臂梁振动传感器[J]. *光学学报*, 2022, 42(15): 1528001.  
Fan J H, Yang X W, Luo B B, et al. Through-hole cantilever beam vibration sensor based on dispersion-turning-point optical microfiber coupler[J]. *Acta Optica Sinica*, 2022, 42(15): 1528001.
- [21] Zhang Z, Pan J, Tang Y, et al. Optical micro/nanofiber embedded soft film enables multifunctional flow sensing in microfluidic chips[J]. *Lab on a Chip*, 2020, 20(14): 2572-2579.
- [22] Liu H T, Song X D, Wang X Y, et al. Optical microfibers for sensing proximity and contact in human-machine interfaces[J]. *ACS Applied Materials & Interfaces*, 2022, 14(12): 14447-14454.
- [23] Leitão C, Antunes P, Pinto J, et al. Optical fiber sensors for central arterial pressure monitoring[J]. *Optical and Quantum Electronics*, 2016, 48(3): 218.
- [24] Castaneda D, Esparza A, Ghamari M, et al. A review on wearable photoplethysmography sensors and their potential future applications in health care[J]. *International Journal of Biosensors & Bioelectronics*, 2018, 4(4): 195-202.
- [25] Huttunen J M J, Kärkkäinen L, Lindholm H. Pulse transit time estimation of aortic pulse wave velocity and blood pressure using machine learning and simulated training data[J]. *PLoS Computational Biology*, 2019, 15(8): e1007259.
- [26] Shahrabaki S S, Ahmed B, Penzel T, et al. Photoplethysmography derivatives and pulse transit time in overnight blood pressure monitoring[C]//2016 38th Annual International Conference of the IEEE Engineering in Medicine and Biology Society (EMBC), August 16-20, 2016, Orlando, FL, USA. New York: IEEE Press, 2016: 2855-2858.
- [27] Smola A J, Schölkopf B. A tutorial on support vector regression [J]. *Statistics and Computing*, 2004, 14(3): 199-222.
- [28] O'Brien E, Mee F, Atkins N, et al. Evaluation of the SpaceLabs 90202 non-invasive ambulatory recorder according to the AAMI Standard and BHS criteria[J]. *Journal of Human Hypertension*, 1991, 5(3): 223-226.
- [29] Xing X M, Sun M S. Optical blood pressure estimation with photoplethysmography and FFT-based neural networks[J]. *Biomedical Optics Express*, 2016, 7(8): 3007-3020.
- [30] Luo H, Yang D Y, Barszczyk A, et al. Smartphone-based blood pressure measurement using transdermal optical imaging technology[J]. *Circulation: Cardiovascular Imaging*, 2019, 12(8): e008857.
- [31] Li L Y, Sheng S F, Liu Y F, et al. Automatic and continuous blood pressure monitoring via an optical-fiber-sensor-assisted smartwatch[J]. *Photonix*, 2023, 4(1): 21.
- [32] Wang J Y, Liu K W, Sun Q Z, et al. Diaphragm-based optical fiber sensor for pulse wave monitoring and cardiovascular diseases diagnosis[J]. *Journal of Biophotonics*, 2019, 12(10): e201900084.
- [33] Chandrasekhar A, Yavarimanes M, Natarajan K, et al. PPG sensor contact pressure should be taken into account for cuff-less blood pressure measurement[J]. *IEEE Transactions on Bio-Medical Engineering*, 2020, 67(11): 3134-3140.
- [34] Bennett A, Beiderman Y, Agdarov S, et al. Monitoring of vital bio-signs by analysis of speckle patterns in a fabric-integrated multimode optical fiber sensor[J]. *Optics Express*, 2020, 28(14): 20830-20844.

## Dual-Channel Reflective Optical Microfiber Coupler Diaphragms for Continuous and Accurate Blood Pressure Monitoring

Zou Xue<sup>1,2</sup>, Fan Junhao<sup>2</sup>, Luo Binbin<sup>2\*</sup>, Zhou Fumin<sup>2</sup>, Wu Decao<sup>2</sup>, Zhang Zufan<sup>1</sup>, Zhao Mingfu<sup>2</sup>

<sup>1</sup>*School of Communication and Information Engineering, Chongqing University of Posts and Telecommunications, Chongqing 400065, China;*

<sup>2</sup>*Chongqing Key Laboratory of Optical Fiber Sensor and Photoelectric Detection, Chongqing University of Technology, Chongqing 400054, China*

### Abstract

**Objective** Cardiovascular disease (CVD) is the most important cause of human death, of which hypertension is the most common chronic disease in people's life and is one of the most important risk factors for CVD. With the socio-economic

development and accelerating population aging and urbanization, hypertension is on the rise. According to research, the presymptoms of hypertension are not obvious, and a considerable portion of patients do not have any uncomfortable clinical symptom such as dizziness, headache, and shortness of breath. When blood pressure is elevated for a long time and exceeds the normal range, this may result in serious complications and even threaten life safety. Therefore, accurate blood pressure monitoring is crucial for early diagnosis and intervention treatment. However, compared with the single point in time blood pressure detection of traditional cuff-type electronic blood pressure monitors, continuous dynamic monitoring can more truly reflect the real-time changes in blood pressure and dynamic trends, providing more comprehensive and accurate data. The human pulse signal contains a large amount of physiological and pathological information related to the cardiovascular system, and continuous blood pressure monitoring can be realized by accurately extracting the characteristic parameters and building a blood pressure prediction model. Currently, the main method of pulse signal detection is the PPG method, whose major drawbacks are high power consumption, sensitivity to ambient light and pressure perturbation, and susceptibility of electronic components to electromagnetic wave interference. As a result, it is impossible to measure blood pressure simultaneously in special environments such as MRI and CT. Thus, we propose a fiber-optic blood pressure sensor with continuous accurate measurement and without spatial alignment based on the microstructural setup of a reflective microfiber coupler, which is achieved by combining dual-channel pulse wave acquisition and machine-learning model prediction. This electromagnetic interference-resistant, wearable, and continuous blood pressure monitoring system will play an important role in human CVD prevention in the future.

**Methods** First, two single-mode fibers twisted around each other are drawn into a microfiber coupler using the flame fusion taper method, and the reflective coupler is formed by cutting flat at the section of the waist region area, which has a diameter of  $5\ \mu\text{m}$  and a length of 10 mm. The device is encapsulated between an epoxy resin substrate and two layers of PDMS circular films, where the substrate is a through-hole structure, the upper PDMS layer is a circular film with a diameter of 15 mm and a thickness of  $100\ \mu\text{m}$ , and the lower PDMS is a raised spherical structure with a diameter of 10 mm and a height of 1.5 mm. Particularly, this structure can improve the detection sensitivity and reduce the sensitivity of the sensing area to the spatial location. Then, a dual-channel pulse wave detection system is set up to obtain the brachial artery transit time (BPTT), the radial artery transit time (RPTT), and the transit time difference between the radial artery and brachial artery (DBRPTT). Finally, the support vector regression algorithm is utilized to build a blood pressure prediction model to realize continuous and accurate blood pressure detection.

**Results and Discussions** The mechanical simulation results of the packaging structure show that it can sense micro-pressure from multiple directions, reducing its dependence on the detection position (Figs. 2–3). In the static pressure experiment, the detection sensitivity is  $-0.682\ \text{kPa}^{-1}$  in the range of 500–1000 Pa. The sensor can respond immediately at the moment of loading and unloading pressure, with the response time of 35 ms and 46 ms respectively. Additionally, the durability and repeatability of the sensor are also tested. After 2500 cycles of the periodic pressure with a frequency of 5 Hz and a size of 1 N, the sensor still shows good response and excellent repeatability. After about 5000 cycles, the response amplitude drops by about 5% from the beginning. Since the time for sensing to measure pulse is short (about five seconds), less impact is exerted on later blood pressure prediction. When the sensor is placed at different positions in the radial artery area, the sensor can effectively detect high-fidelity pulse signals, indicating that there are no strict alignment requirements between the sensor and the artery (Fig. 5). By employing a dual-channel sensing system, the pulse waveforms at the radial artery and brachial artery are collected simultaneously. Three PTT (BPTT, RPTT, and DBRPTT) characteristic parameters (Fig. 6) are extracted from these sample data to build a blood pressure prediction model. The correlation diagram and Bland-Altman diagram reveal that both the true and the predicted values are negatively correlated with the  $K$  value. The correlation coefficient  $R$  values of SBP and DBP are 0.96 and 0.95 respectively, which indicates that there is a good positive correlation between the reference and predicted values. The mean difference value and SD value of SBP are 0.08 mmHg and 1.13 mmHg respectively, and the mean difference value and SD value of DBP are  $-0.35\ \text{mmHg}$  and 1.25 mmHg respectively (Fig. 11). These indicators are both lower than the AAMI standard  $[(5\pm 8)\ \text{mmHg}]$ . The performance comparison results between the sensor and other blood pressure sensors show that the sensor features an extremely compact structure, high sensitivity, sound stability, long service life, and anti-electromagnetic interference. Finally, a volunteer is randomly selected to collect 14 sets of data from 8:00 to 21:00 a day to verify the feasibility of the sensor. The results demonstrate that the normal pattern of “two peaks and one trough” is blood pressure trends. Another volunteer receives continuous monitoring during a mixed exercise of squatting and jogging. As the exercise time increases, both SBP and DBP rise but remain stable after about ten minutes (Fig. 12). This shows that the proposed blood pressure monitoring system can continuously and effectively monitor the health level of blood pressure.

**Conclusions** We develop a reflective optical microfiber coupler sensor chip (R-OMCSC) for cardiovascular health assessment of accurate and continuous blood pressure monitoring. The R-OMCSC exhibits performance with high

sensitivity and detection pulse wave without spatial alignment, which allows for perceiving weak physiological signals. Embedding the sensor into a sports wristband, we construct a dual-channel pulse wave detection system, obtain the RPTT, DPTT, and DBRPTT values, and build an SVR prediction model. Experimental results show that the system can achieve continuous blood pressure monitoring. In the future, we will keep improving the integration of the photoelectric signal processing system with the proposed dual-channel R-OMCSC pulse wave sensor, and a large amount of data will be collected for more accurate analysis. The proposed non-invasive BP detection system features high accuracy and continuous monitoring and will have the opportunity to be employed for clinical applications and thus help patients with CVD prevention.

**Key words** sensors; blood pressure monitoring; micro-nano fiber coupler; human pulse wave; support vector regression